

Electronic Supplementary Information (ESI)

Plasmonic Gratings with Nano-protrusions Made by Glancing Angle Deposition for Single-Molecule Super-Resolution

*Biyang Chen^{a,‡}, Aaron Wood^{b,‡}, Avinash Pathak^a, Joseph Mathai^a, Sangho Bok^a, Haisheng
Zheng^a, Steven Hamm^a, Sagnik Basuray^a, Sheila Grant^b, Keshab Gangopadhyay^a, Peter V.
Cornish^{c,*}, Shubhra Gangopadhyay^{a,*}*

a Department of Electrical and Computer Engineering, 139 and 141A Engineering Building
West, University of Missouri, Columbia, MO 65211 (USA)

b Department of Bioengineering, 139 and 141A Engineering Building West, University of
Missouri, Columbia, MO 65211 (USA)

c Department of Biochemistry, 117 Schweitzer Hall, University of Missouri, Columbia, MO
65211 (USA).

* Corresponding author e-mail: S. Gangopadhyay (gangopadhyays@missouri.edu); P. V.
Cornish (cornishp@missouri.edu).

1. Deposition and Morphology

1.1 GLAD growth process and AFM for GLAD gratings with rapid or stepped silver deposition rates

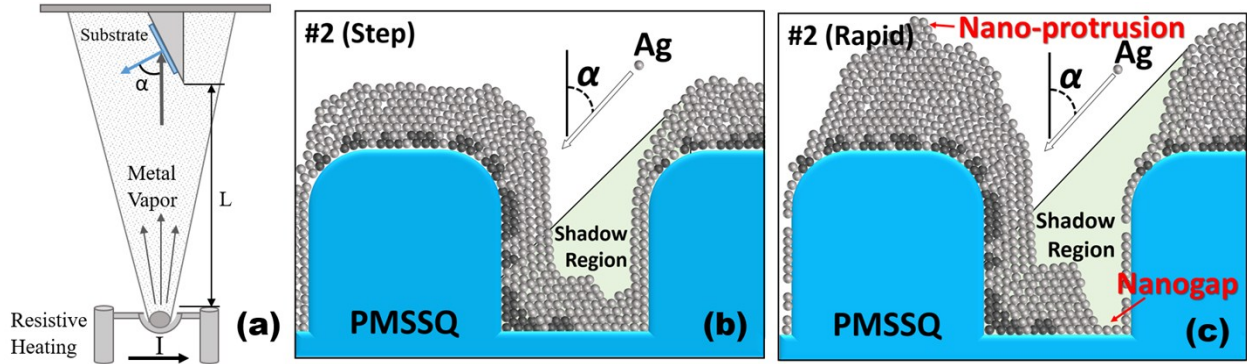


Figure S1 (a) GLAD growth process showing the oblique arrival of silver vapor to the PMSSQ gratings; Illustration of the GLAD growth process showing the oblique arrival of silver vapor to the PMSSQ gratings (supplementary to the main paper): (b) step #2. Stepped deposition encourages lateral growth resulting in smaller nanogaps and fewer nano-protrusions; (c) step #2. Rapid silver deposition encourages vertical growth that results in plenty of nano-protrusions, large nanogaps on the grating walls.

1.2 AFM for silver GLAD gratings deposited at different angles

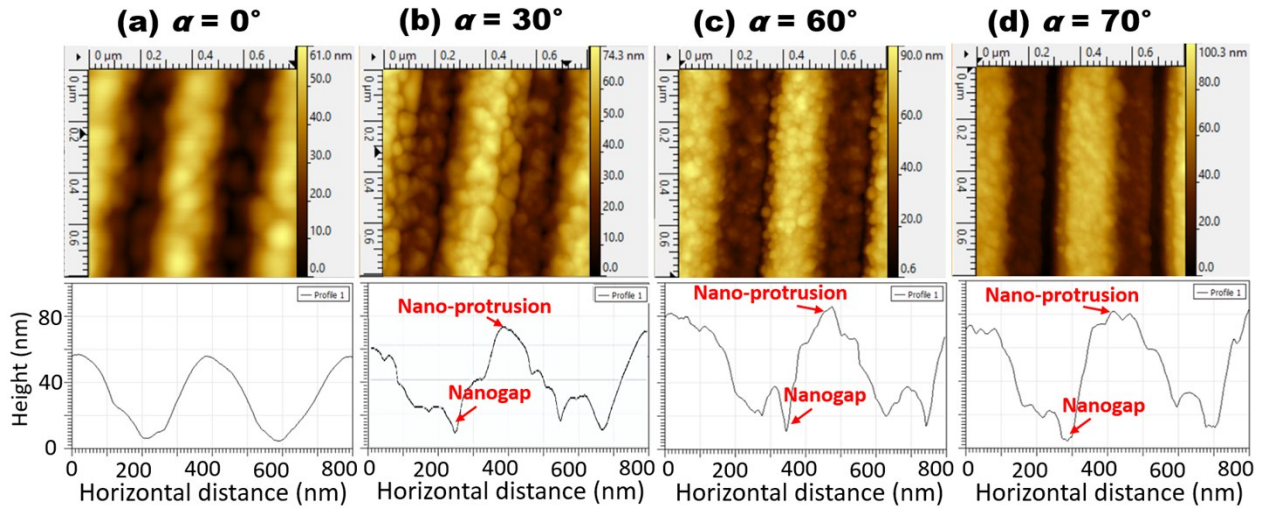


Figure S2 2D AFM images and profiles of silver GLAD gratings with rapid silver deposition rates at different deposition angles (a) $\alpha = 0^\circ$, (b) $\alpha = 30^\circ$, (c) $\alpha = 60^\circ$, (d) $\alpha = 70^\circ$.

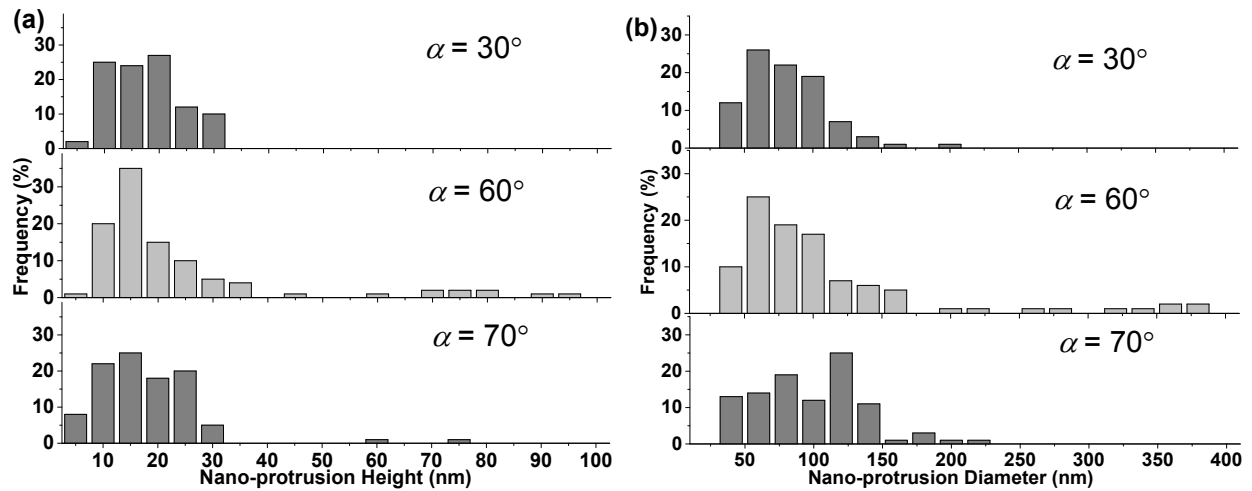


Figure S3 (a) Nano-protrusion height above the grating ridge histograms and (b) nano-protrusion base diameter histograms at $\alpha = 30^\circ$, $\alpha = 60^\circ$, and $\alpha = 70^\circ$ deposition angles. Histograms obtained from a sample of 100 nano-protrusions from AFM topography scans with a ~ 1 nm radius tip. GLAD samples were deposited over an 8 month period and found to be very consistent in surface structure and reflectance.

1.3 AFM to show different nanostructures in silver GLAD gratings

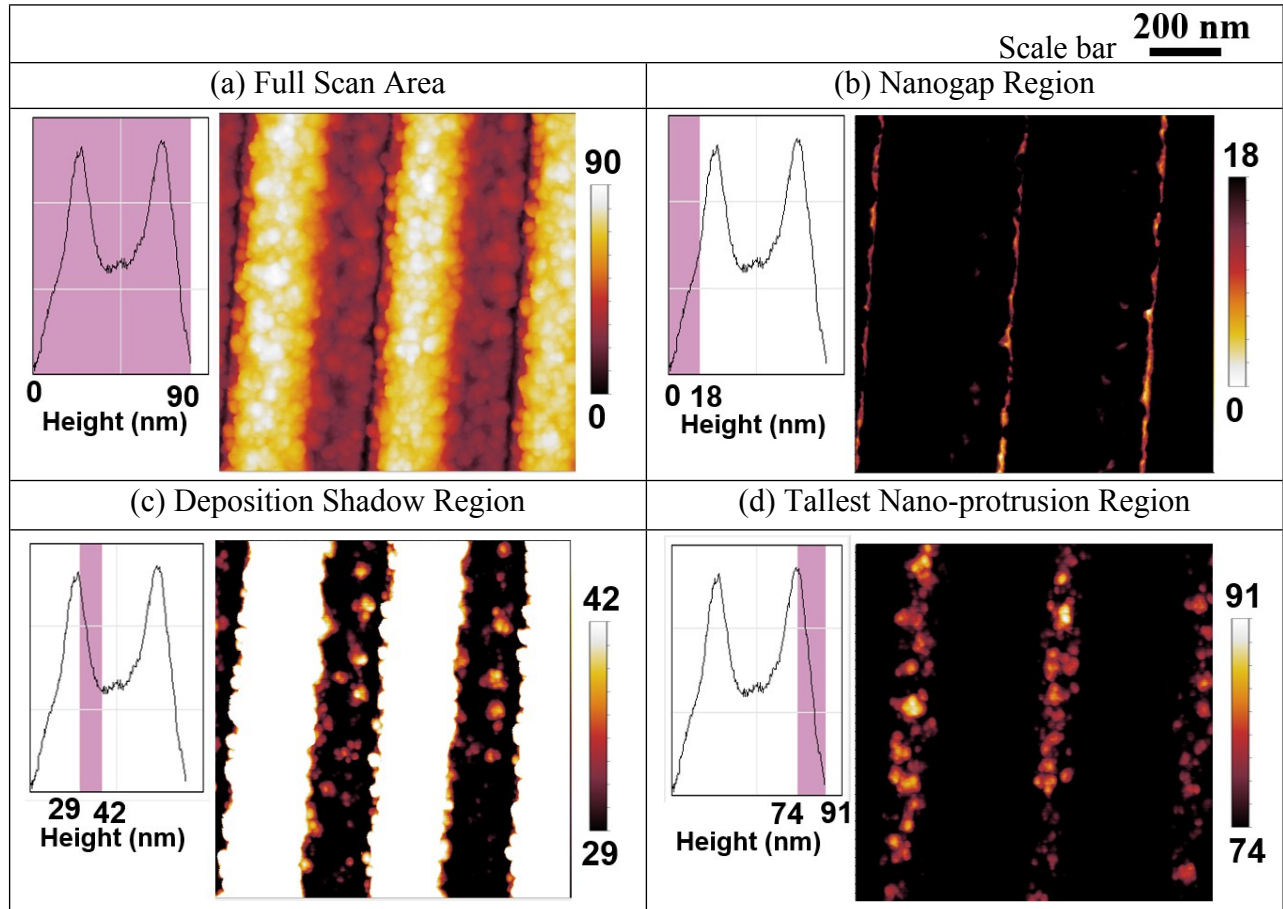


Figure S4 $1 \times 1 \mu\text{m}$ AFM scans and height histograms of silver GLAD gratings ($\alpha = 60^\circ$) with the (a) entire scan or (b,c,d) regions of interest highlighted. Highlighted portion of the GLAD grating containing the (b) nanogap region, (c) nano-protrusions in the deposition shadow region, and (d) Nano-protrusion region on top of the grating ridge.

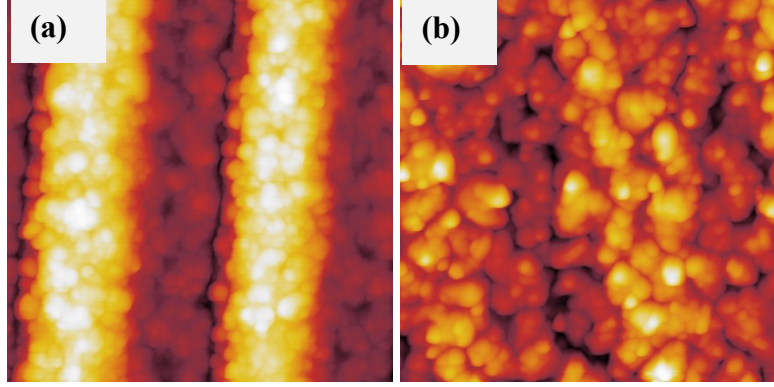


Figure S5 800×800 nm AFM scans of (a) 60° GLAD Grating and (b) silver grown on flat glass deposited at 60° GLAD with the same height scale as Fig. S2 (0 – 90 nm). Scanned with a ~1 nm AFM tip. The roughness of the flat silver film and its granular structure provides a substantial increase in surface area as compared to, for example, glass surfaces. The calculated surface area via Gwiddyon © AFM analysis software of (a) is $782.475 * 10^{-15}m^2$ with a projected flat area of $640.0 * 10^{-15}m^2$. (b) has a calculated surface area via via Gwiddyon © of $782.173 * 10^{-15}m^2$ and a projected flat area of flat area of $640.0 * 10^{-15}m^2$.

2. Experimental and Simulated Optical properties

2.1 Experiment and Simulation for reflectance and E-field of GLAD and regular gratings in air

Using Maxwell's equations, we can determine the wave vector matching conditions for a particular metal grating and dielectric interface using **Equation S1**.¹

$$k_{SPP} = \frac{\omega}{c} \sqrt{\frac{\epsilon_m \epsilon_d}{\epsilon_m + \epsilon_d}} = k_{ph}^x \pm mG \quad (m = \pm 1, 2, 3, \dots) \quad (S1)$$

Where k_{SPP} is the wave vector of the SPP, $k_{ph}^x (= \frac{\omega}{c} \sqrt{\epsilon_d} \sin\theta)$ is the incident transverse wave vectors, $G = \frac{2\pi}{\Lambda}$ is the grating vector represents the additional wave-vector gained through diffractions where Λ is pitch or spacing of the grating and m is an integer representing the diffraction order; ω is the frequency of the incident light, θ is incident angle, ϵ_m is the dielectric constant for the metal, and ϵ_d is the dielectric constant for the medium surrounding the metal. The matching conditions described in this equation can be explored using experimental data from a silver GLAD grating. The ability to couple light at specific pairs of wavelengths and angles of incidence demonstrates that SPR can only form at intersections between the SPP wave vector and the light line ($k_{ph} \sin\theta$).²

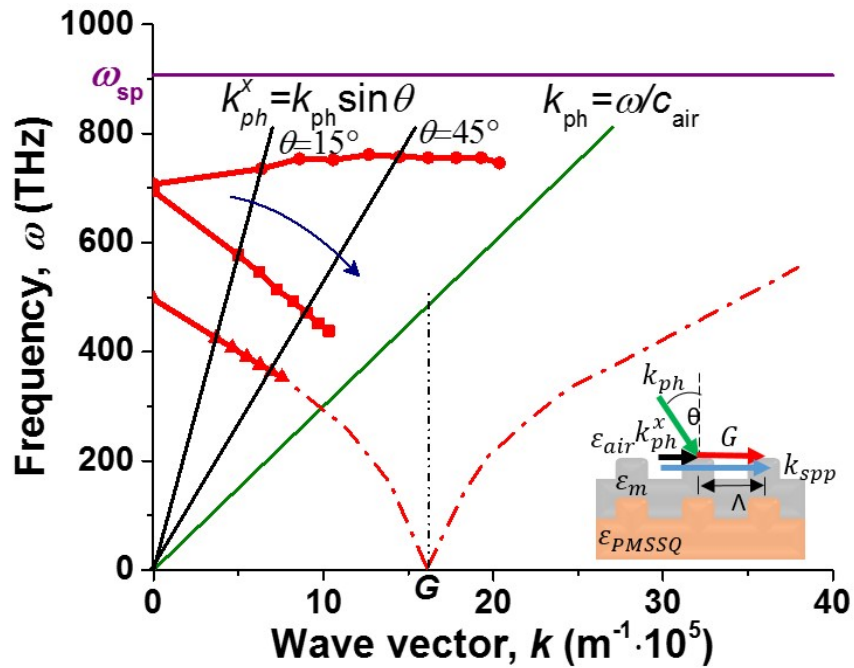


Figure S6 Experimental frequency vs. wave vector plot for a silver GLAD grating in air calculated by the SPR peak location from the reflectance. Inset: Illustration of the wave vector matching between incident EM radiation (transverse-magnetic (TM) light) on a grating and a propagating surface plasmon polariton.

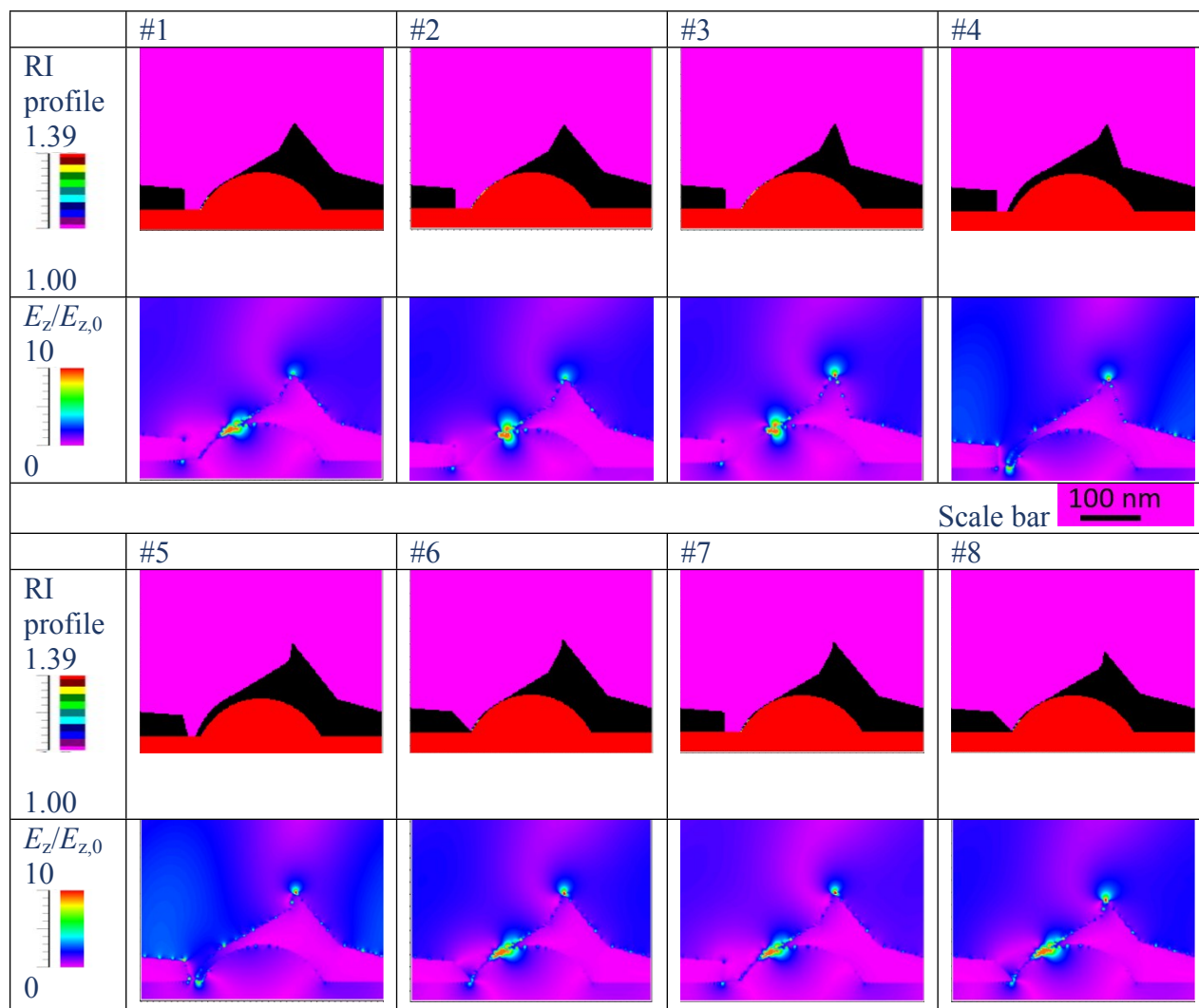


Figure S7 Design of simulated geometry for 40 nm Ag HD-DVD GLAD gratings: refractive index (RI) profile and E-field ($E_z/E_{z,0}$) at 40° incident angle at resonance wavelength in air; intensity bar is 0-10, and scale bar is 100 nm.

We performed 2D finite-difference time-domain (FDTD) simulations in this work and various geometries were simulated to provide a better understanding of the influence of each shape on the E-field concentration. First, a basic modeling geometry was built with the structural information provided by the high resolution (~ 1 nm tip) AFM results seen in **Fig. S2** and **S4**. Then, we tested several structures (the 8 geometries in **Fig. S7** are examples) by modifying different nano-protrusion parameters (height, width, sharpness), nanogap widths and thickness of

shadowed regions, etc. The contour maps of refractive index illustrate the morphology and size of the silver and PMSSQ gratings. The nano-protrusion was built from several triangles and rectangles to achieve the desired morphology. As illustrated in **Fig. S7**, sharper nano-protrusions (#3-8) are able to concentrate more energy at the tips resulting in a higher E-field at the tips than smoother nano-protrusions (#1-2). The thinner shadowed regions tend to form additional hot-spots at the interface of silver and PMSSQ, which results in an additional reflectance dip at longer wavelengths. Structure #8 was ultimately chosen as it had the closest match in reflectance and hot spot position as the experimental 60° GLAD gratings. This structure was then used to model E-field and reflectance intensity for different conditions such as a PMSSQ coating on top, aqueous environment, etc.

The simulation matches with experiment quite well by showing additional GLAD reflectivity dip in approximately 800 nm of wavelength with 40° incident angle. **Fig. S8** shows the simulated E-field distribution at the cross-section of GLAD gratings. In the visible region, E-field is highly concentrated at the nanocones and nanopurs while other areas on the grating surface show very low E-field.

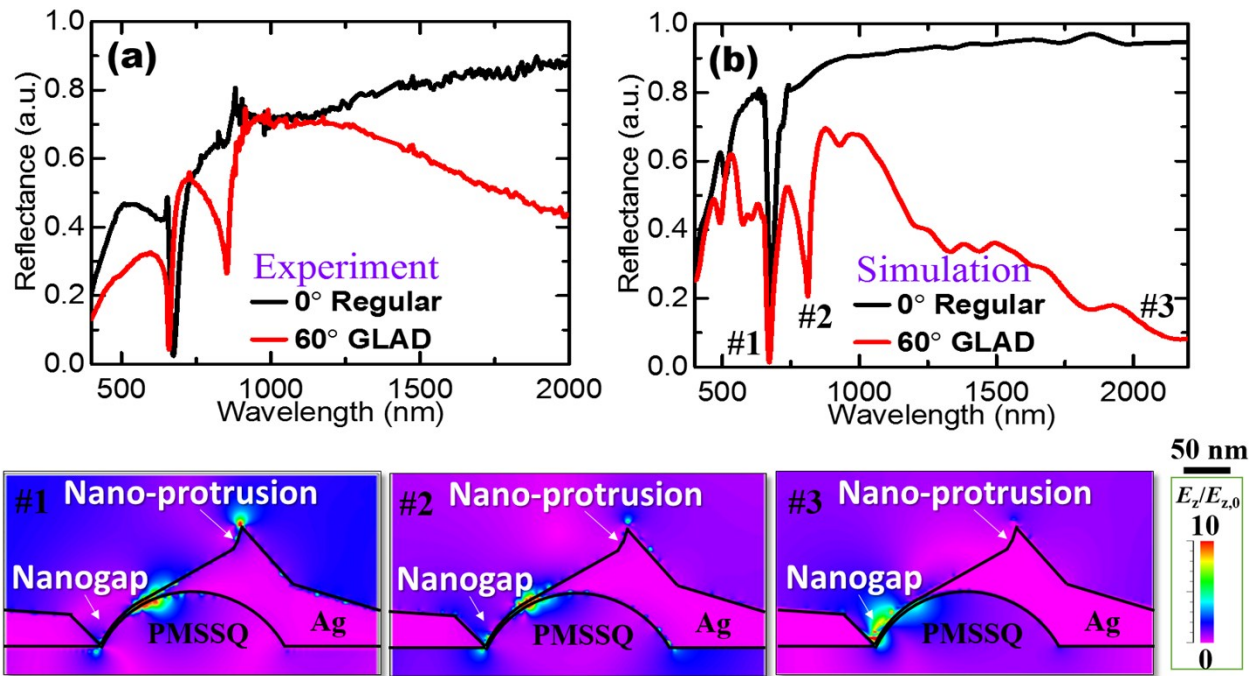


Figure S8 Experimental and simulated p-polarized light reflectance spectra taken at 40° incidence of 40 nm Ag gratings deposited at $\alpha = 0^\circ$ (regular) and $\alpha = 60^\circ$ (GLAD) in air; (#1-#3) FDTD-simulated E-field ($E_z/E_{z,0}$) for one period of GLAD structure showing E-field concentration at hot spots for different incident wavelengths; intensity bar is 0-10, and scale bar is 50 nm.

2.1 Experiment for reflectance of GLAD and regular gratings in air

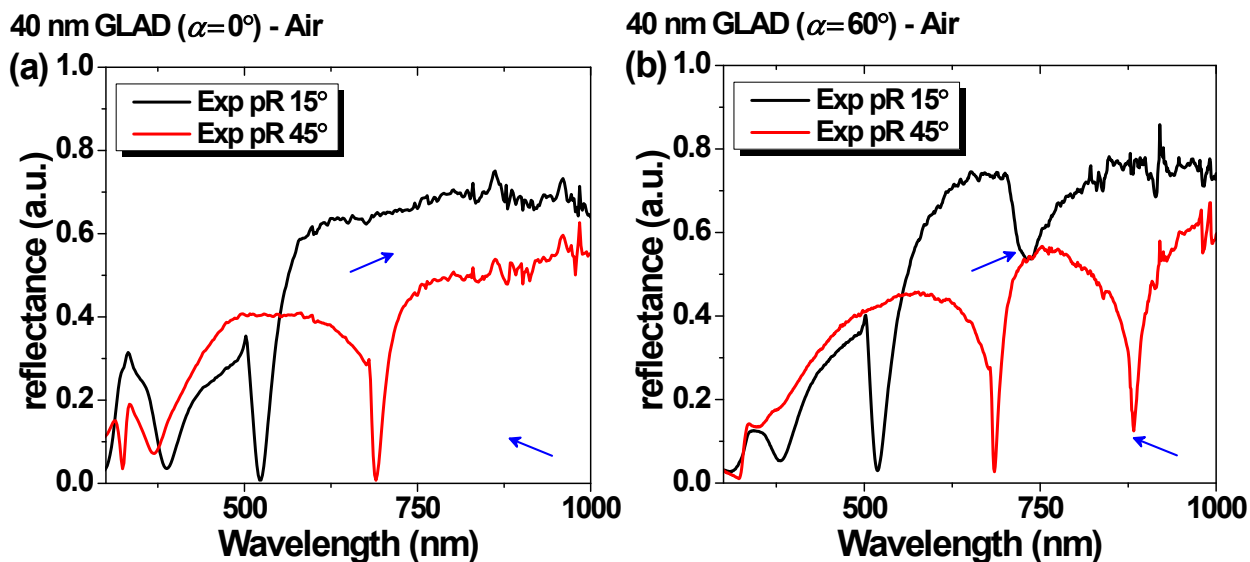
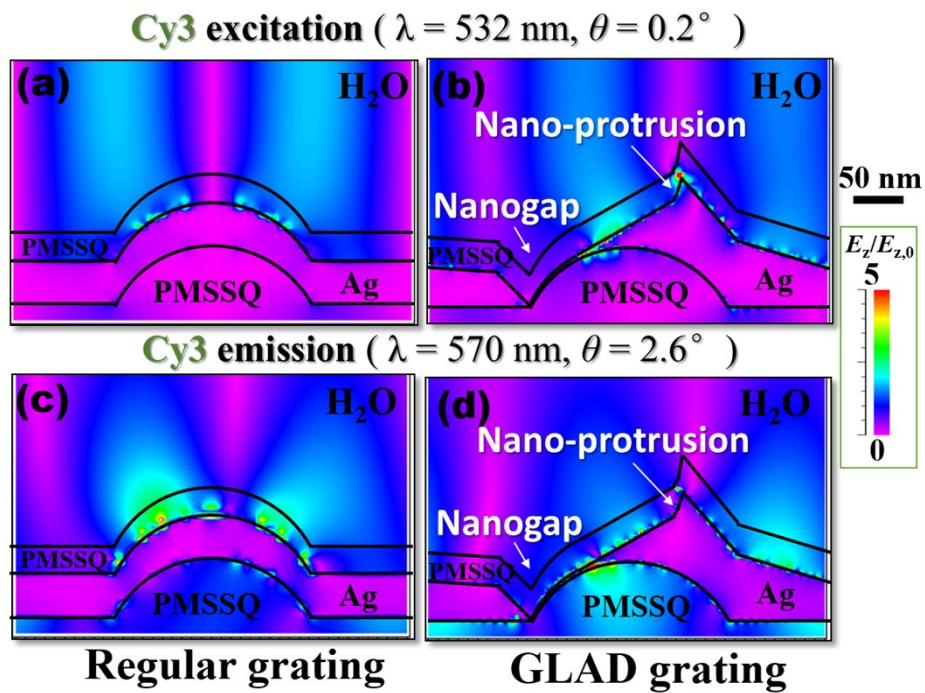


Figure S9 Experimental reflectance taken by ellipsometry for 40 nm silver HDDVD gratings: (a) regular grating ($\alpha = 0^\circ$) in the air, (b) GLAD grating ($\alpha = 60^\circ$) in the air. The blue arrows point out the additional peak from GLAD gratings compared with regular gratings.

For Cy3 excitation with laser wavelength at 532 nm, the highest localized E-field at a hot spot is achieved at $\theta = 0.2^\circ$, showing highly localized E-field at nano-protrusion (**Figure S10b**). However, the regular grating (**Figure S10a**) under this condition does not couple the light into PMSSQ/silver interface to form an evanescent wave. Therefore, instead of SPR coupling, LSPR coupling plays a main role in the E-field enhancement at hot spots. For Cy3 emission with fluorescence peak at $\lambda = 570$ nm, hot spots shows highest E-field at $\theta = 2.6^\circ$ (**Figure S10d**). SPR coupling with “bunny ear” shape (typical shape of E-field for higher frequency resonance mode^{3,4}) is formed under this circumstance for regular grating (**Figure S10c**). Owing to the E-field mainly coupled at two wedges on top of gratings under this resonance mode, the evanescent

wave formed by SPR coupling is further concentrated at nano singularities including nano-protrusion and nanogap region for GLAD gratings. The simulated maximum E-field for Cy5 excitation and emission is greater than that for Cy3, which is consistent with the experimental observation that Cy5 shows higher fluorescence enhancement than Cy3. The excitation wavelength of Rhodamine 6G (R6G) dye is the same as Cy3. Moreover, the emission wavelength of R6G is 570 nm.



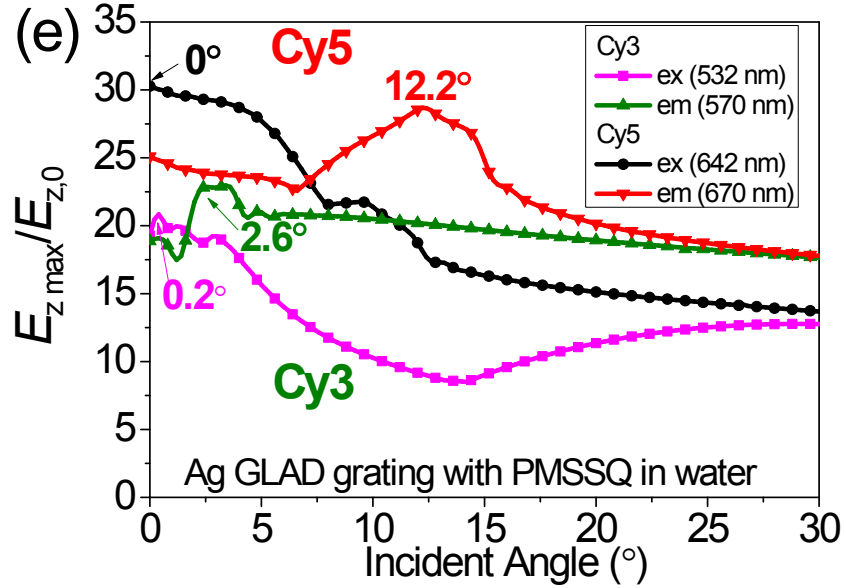


Figure S10 Simulated E-field ($|E_z/E_{z,0}|$) distribution for 40 nm Ag regular (left) and GLAD (right) gratings coated with 30 nm PMSSQ in water environment at excitation and emission wavelength of Cy3: (a, b) Cy3 excitation ($\lambda = 532$ nm, $\theta = 0.2^\circ$); (c, d) Cy3 emission ($\lambda = 570$ nm, $\theta = 2.6^\circ$). Intensity bar is 0-5, and the scale bar is 50 nm. (e) Simulated maximum $E_z/E_{z,0}$ at hot spots vs. incident angle for 40 nm Ag GLAD gratings coated with 30 nm PMSSQ in water environment at excitation and emission wavelength of Cy3 and Cy5. The angles with the maximum $E_z/E_{z,0}$ are as indicated.

3. Fluorescence enhancement for Cy5 on GLAD grating

3.1 Effect of deposition angles

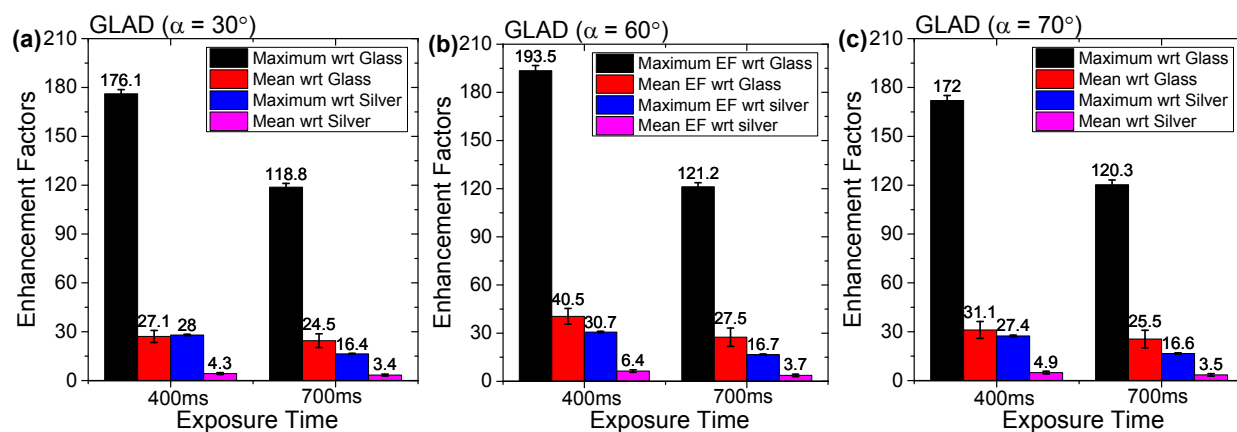


Figure S11 Enhancement factors (with respect to glass and flat silver) with spun-coated Cy5 (in PMSSQ + ethanol solution) on 40 nm silver HDDVD GLAD gratings at different deposition angles (a) $\alpha = 30^\circ$, (b) $\alpha = 60^\circ$, (c) $\alpha = 70^\circ$. The images were taken with 60 \times water-immersion objective and with 400 ms and 700 ms exposure times. The samples were illuminated by Xenon light source with broad spectra filtered by Cy5 filter cubes.

3.2 Effect of metals for gratings

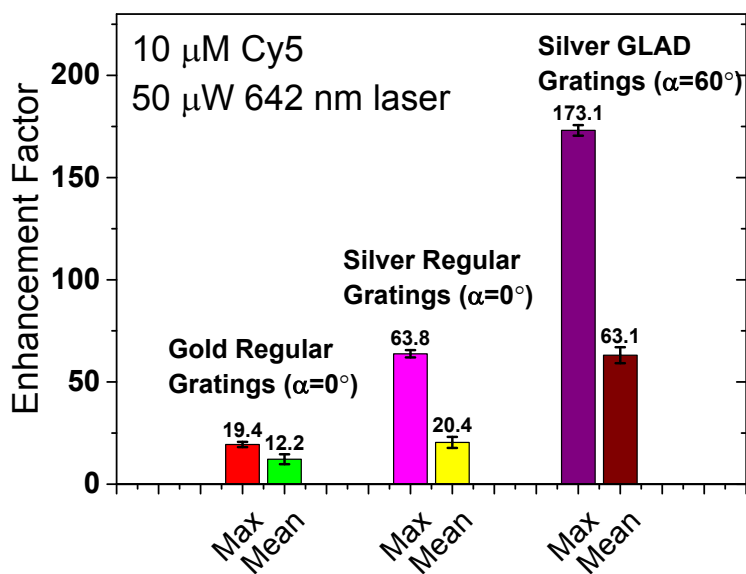


Figure S12 Enhancement factors for Cy5 on different substrates. All measurements were performed using a 60 \times water-immersion objective, with 10 μ M Cy5 dye in ethanol spun coated

on the substrates. The enhancement factors were calculated with respect to the plain glass slides and the incident laser power was fixed at 50 uW on all the substrates. The camera gain was also fixed at 1 and the integration time was 100ms. Gold gratings are deposited with 100nm gold on PMSSQ gratings while silver gratings have a 100nm layer of silver deposited by sputtering. The GLAD gratings have a 40nm layer of thermally deposited silver.

4. Gold Coatings and Fluorescence Enhancements

The gold film thickness was selected to be 10 nm to produce a semi-conformal coating for DNA attachment but not thick enough to substantially reduce the plasmonic field strength. The simulated structure is based on a 30 nm silver grating deposited by GLAD method and sequentially a 10 nm layer of silver or gold coating conformally deposited on the surface of GLAD grating. Therefore, the surface morphology is the same for these two coatings, which can avoid the effect of different GLAD structures on E-field distribution. In both cases, there are mainly two levels of hot-spots: highest E-field is concentrated at nano-protrusion and the second highest E-field is located at nanogap.

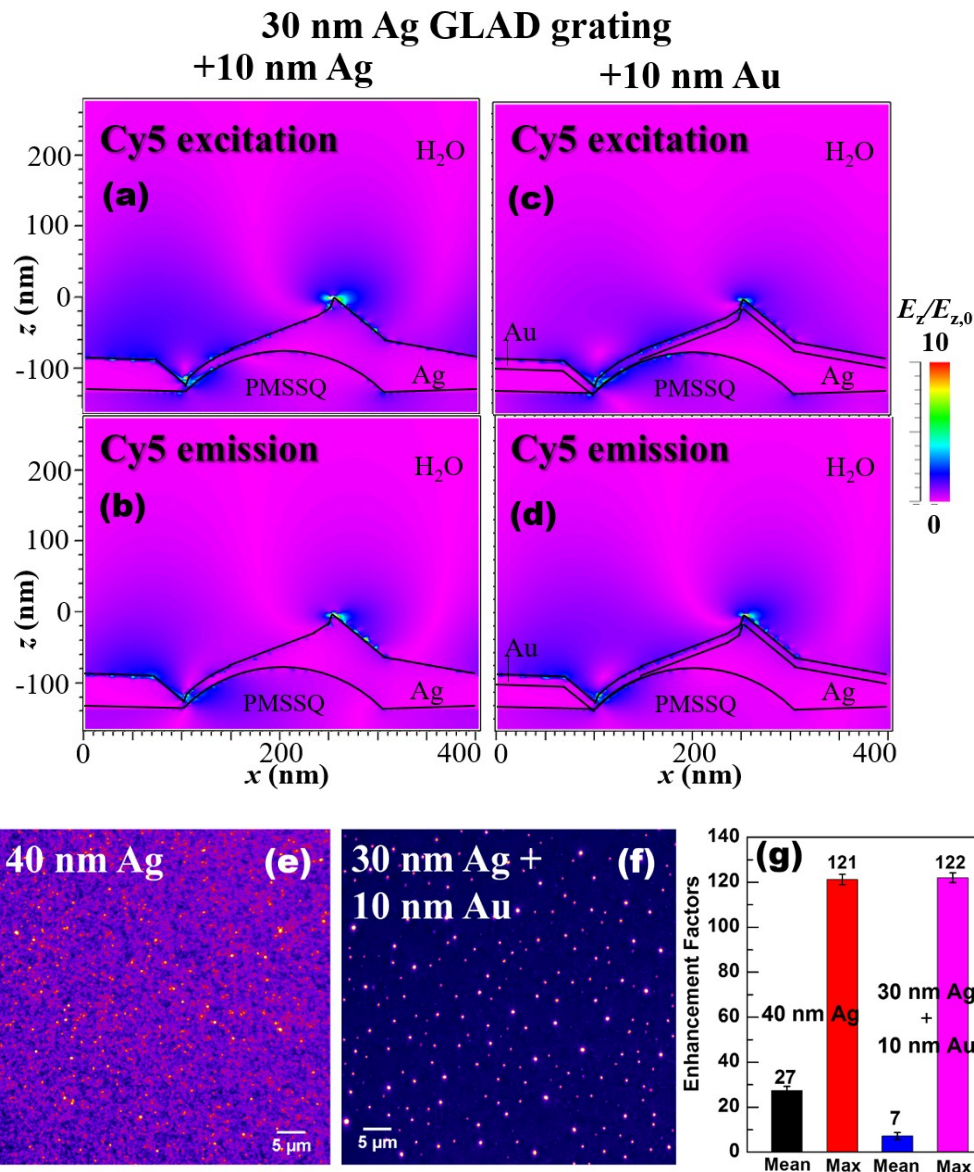


Figure S13 Effect of Au coating on E-field and fluorescence. Simulated E-field distribution for 30 nm Ag GLAD grating with additional (a, b) 10 nm Ag and (c, d) 10 nm Au coating at excitation and emission wavelength of Cy5 taken at 0° incidence in water. E-field strength is plotted from 0 to 10. Note: Cy5 excitation wavelength = 642 nm, Cy5 emission wavelength = 670 nm. Fluorescence images (false-color) for (e) 40 nm Ag and (f) 30 nm Ag + 10 nm Au GLAD grating ($\alpha = 60^\circ$) with 10 μM Cy5 in 30 nm PMSSQ coating; (g) corresponding mean and maximum enhancement factors with respect to the glass with 700 ms exposure time.

Gratings fabricated using a GLAD of 30 nm silver at an angle of 60° with respect to horizontal and then deposited with 5 nm or 10 nm gold were checked for their stability in a T50 buffer solution. To do so, a 200 μ l volume of T50 solution was dropped on the surface of the gratings and surrounding silver and left inside a closed Petri-dish overnight. The gratings were then blow dried with nitrogen and imaged under the microscope. A tape test was performed after the overnight period to ensure adhesion.

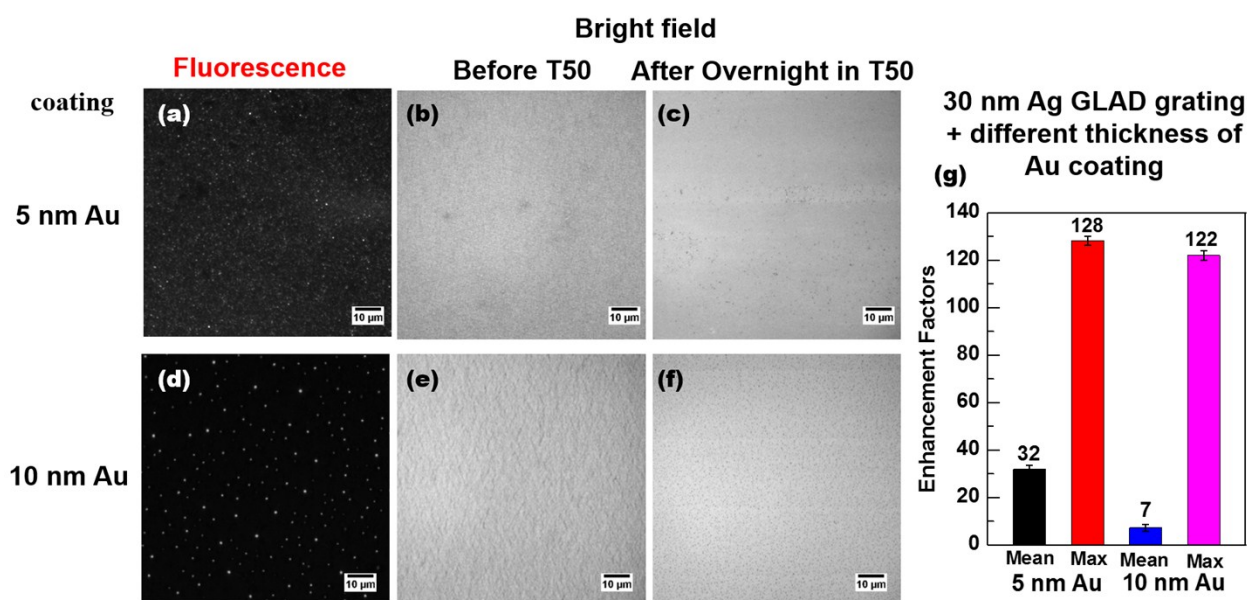


Figure S14 Fluorescence and bright field images for 30 nm Ag GLAD grating ($\alpha = 60^\circ$) capped with different thickness of gold (a-c) 5 nm and (d-g) 10 nm, with 10 μ M Cy5 in 30 nm PMSSQ coating. Bright field images: (b, e) before and (c, f) after T50 buffer solution overnight test. The scale bar for all images is 10 μ m. (g) Corresponding mean and maximum enhancement factors with respect to the glass with 700 ms exposure time.

5. Imaging Single-Molecule for DNA-RNA duplex on GLAD Grating using Epifluorescence Microscope

5.1 AFM topography locations vs. Fluorescence Images

The vast majority of fluorescent spots observed at the high and low intensity on the nano-protrusions exhibit single step bleaching which indicates that the individual molecules are located on or near the apex of each nano-protrusion. Locating the exact location of the $10\mu\text{m} \times 10\mu\text{m}$ AFM scan in fluorescence microscopy has proved very difficult, especially at lower/single molecule concentrations where the dye molecules are bleaching while searching for the AFM scan location. We have attempted marking/scratching of the grating before AFM for faster location searching but this lead to faster degradation of the silver film around the scratch location in biological buffers and non-uniformity in the PMSSQ film thickness after spinning dye coatings.

We have thus selected the most similar fluorescence image as the AFM scan that we could find on the same sample, and the population of smaller and larger nano-protrusions appears to correlate with the population of smaller and larger spot intensities. Based on our simulations, larger and sharper nano-protrusions better concentrate the plasmonic field than smaller and it is well understood that higher EM field intensity at the apex of the nano-protrusion is directly related to the intensity of the fluorescence dye emission as seen in Das, et. al.

5.2 Rayleigh diffraction limit

The observation of sub-wavelength structures with microscopes is limited by diffraction limit for general system:

$$d = 0.61 \frac{\lambda}{NA} \quad (S2)$$

Where d is the Rayleigh diffraction limit, λ is the wavelength of light, NA is the numerical aperture of the objective lens.

Table S1 The Rayleigh diffraction limit (in nanometers) given different wavelengths and different objective lenses.

Wavelength (nm) \ Objective Lens	Cy3 excitation 530	R6G emission 550	Cy3 emission 570	Cy5 excitation 642	Cy5 emission 670
60× water (NA = 1.2)	270	279	290	327	340

Note: R6G is rhodamine 6G dye.

5.3 Fluorescence images for 50 pico-Molar Cy3/Cy5 labeled DNA/RNA duplex

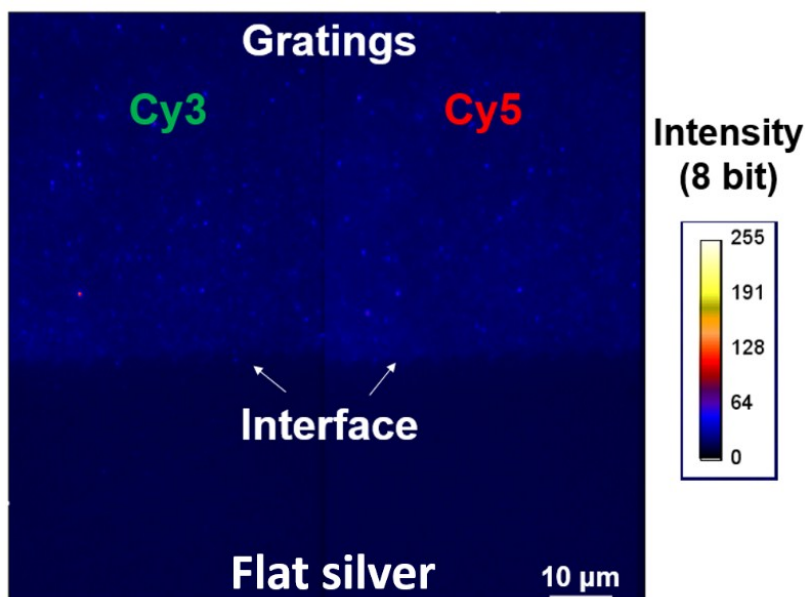


Figure S15 Fluorescence image of 50 pM Cy3/Cy5 labeled DNA/RNA duplex (helicase) immobilized on 40 nm silver GLAD grating ($\alpha = 60^\circ$) platform including grating region and flat silver region: (left) Cy3 channel and (right) Cy5 channel. 14 mW 532 nm green laser was used to

excite Cy3. It shows there is fluorescence enhancement of GLAD grating compared with flat silver, especially at hot-spots.